Chapter II:
MAGNETIC FIELDS - GENERATION, ACTIVITY, AND INSTABILITIES

https://doi.org/10.1017/S1743921322004665 Published online by Cambridge University Press

The IAUS372 audience listening to the review talk by T. Li (China) on CMEs and flares, August 2, 2022.

https://doi.org/10.1017/S1743921322004665 Published online by Cambridge University Press

The Era of Multi-Messenger Solar Physics
Proceedings IAU Symposium No. 372, 2023
G. Cauzzi & A. Tritschler, eds.
doi:10.1017/S1743921322004665

Solar flare-CME association

Ting Li[1,2]

[1]National Astronomical Observatories, Chinese Academy of Sciences, Beijing 100101, China; liting@nao.cas.cn

[2]School of Astronomy and Space Science, University of Chinese Academy of Sciences, Beijing 100049, China

Abstract. We carry out the first statistical study that investigates the flare-coronal mass ejections (CMEs) association rate as function of the flare intensity and the total unsigned magnetic flux (Φ_{AR}) of ARs that produces the flare. Our results show that flares of the same GOES class but originating from an AR of larger Φ_{AR}, are much more likely confined. This implies that Φ_{AR} is a decisive quantity describing the eruptive character of a flare, as it provides a global parameter relating to the strength of the background field confinement. We also calculated the mean twist values α in regions close to the polarity inversion line and proposed a new parameter $\alpha/\Phi_{\rm AR}$ to measure the probability for a large flare to be associated with a CME. We find that the new parameter $\alpha/\Phi_{\rm AR}$ is well able to distinguish eruptive flares from confined flares.

Keywords. Sun: activity, Sun: flares, Sun: coronal mass ejections (CMEs), Sun: magnetic fields

1. Introduction

Solar flares are sudden, localized brightenings of the solar atmosphere evident throughout the entire electromagnetic spectrum and often occur in association with coronal mass ejections (CMEs). During these solar activities, a vast amount of magnetic energy is released, converted into particle acceleration, kinetic energy and plasma heating (Fletcher et al. 2011). According to whether solar flares are associated with CMEs, they can be divided into two types, "eruptive flares" associated with a CME and "confined flares" not associated with a CME. Statistically, the percentage of flares associated with CMEs increases with the strength of the flare, with the strongest X-class flares almost always associated with a CME (Yashiro et al. 2006). Understanding the association between flares and CMEs is important to forecast space weather in the near-Earth environment and meanwhile, the solar flare-CME paradigm might be applied to magnetic activities in other stars, which is vital for the question of exoplanet habitability and the evolution of stellar mass loss and rotation (Lammer et al. 2007).

Two factors are typically suggested to define whether a flare would be eruptive or confined. The first factor describes the active region (AR) non-potentiality, i.e., magnetic helicity, free magnetic energy, twist, etc. (Liu et al. 2016; Toriumi et al. 2017). Recently, Gupta et al. (2021) found that the AR is likely to produce large CME-associated flares if the relative contribution of free magnetic energy, the fraction of non-potential helicity and the normalized current-carrying helicity are larger than certain thresholds. Avallone & Sun (2020) and Kazachenko et al. (2022) found that confined ARs tend to be more current neutralized than eruptive ARs. The second factor describes the constraining effect of the overlying field: its decay rate with height and strength (Sun et al. 2015; Amari et al. 2018). Wang & Zhang (2007) and Baumgartner et al. (2018) found that confined events often occur closer to the magnetic center of ARs, while eruptive events

tend to occur close to the edge of ARs. The decay index, which is derived from magnetic field extrapolations, describes how fast the constraining magnetic field decays and, thus, determines whether a full eruption could take place or not (Török & Kliem 2005). A faster decrease, i.e., higher decay index, reflects more favourable conditions for eruptive flares (Wang et al. 2017; Vasantharaju et al. 2018).

2. Summary of our results

Based on the *Solar Dynamics Observatory* (*SDO*; Pesnell et al. 2012) observations, we established a database including a total of 322 flares (170 eruptive and 152 confined) of Geostationary Operational Environmental Satellite (*GOES*) class M1.0 and larger that occurred within 45° from the central meridian, from June 2010 until June 2019 (see detailed description in Li et al. 2020). For each event, we obtained these GOES parameters from the GOES soft X-ray (SXR) (1-8 Å channel) light curve: 1. FWHM of the light curve, Duration (FWHM); 2. e-folding decay time, Duration (decay); and 3. peak flux, F_{SXR}. Duration (decay) was obtained from the time derivative of the GOES 1-8 Å flux, and defined as the period when the derivative is above 1/e of the maximum value (Song & Tian 2018).

The AR parameters are obtained by using the available vector magnetograms from Space-Weather HMI AR Patches (Bobra et al. 2014) before the flare onset. Total AR magnetic flux, AR area and normalized field strength, which is the total AR flux normalized by the AR area, are calculated for each event by considering all pixels of $|B_r|$>100 G. Four ribbon parameters are calculated for each event, including the ribbon area, total unsigned flux inside the ribbon (obtained from the RibbonDB catalog in Kazachenko et al. 2017), normalized field strength of the ribbon and ribbon distance. In Figure 1, we give an example of a confined M2.7-class flare on 2013 October 23, which initiated at 20:41 UT and peaked at 20:53 UT. We extracted the flare ribbons from 1600 Å images (Figures 1(a)-(b)) by defining them as the pixels with intensity at any time during the flaring (from the flare start time to the end time) equal to or larger than 40σ (standard deviation) above the mean of the quiet-Sun values, and we made composite AIA 1600 Å flare ribbons (Figure 1(c)). The separation between the two area-weighted centroids of the composite ribbons in the positive and negative polarities is obtained as the parameter of ribbon distance (Figure 1(d)). The FWHM duration of the GOES light curve for this event is about 670 s (Figures 1(e)-(f)).

Figure 2 displays the histograms of GOES parameters, AR parameters and ribbon parameters for confined (red lines) and eruptive (blue lines) events. As seen from Figures 2(a1)-(a2), there are slight differences in distributions of Duration (FWHM) and Duration (decay) between the confined and eruptive cases. The averages of the log values of Duration (FWHM) are 652 s (indicated by vertical dotted red line in panel (a1)) and 772 s (vertical dotted blue line) for confined and eruptive cases (difference=17%, hereafter we use relative difference |a-b|/(|a+b|/2) to show the quantitative difference between a and b), respectively. The averages of the log values of Duration (decay) are 1122 s (indicated by vertical dotted red line in panel (a2)) and 1360 s (vertical dotted blue line) for confined and eruptive cases (difference=19%), respectively. The histogram of GOES peak flux F_{SXR} shows that the number of confined flares is more than eruptive flares for <M2.0-class flares and that of confined flares is less than eruptive flares for >M2.0-class (panel (a3)).

For AR parameters, there are significant differences in distributions of AR magnetic flux and AR area between the confined and eruptive cases (panels (b1) and (c1)). The confined events have larger AR magnetic flux and AR area. The averages of the log values of Φ_{AR} (indicated by vertical dotted lines) are 6.5×10^{22} Mx and 4.4×10^{22} Mx for confined and eruptive cases (difference=39%), respectively. The log-mean values of AR area for

https://doi.org/10.1017/S1743921322004665 Published online by Cambridge University Press

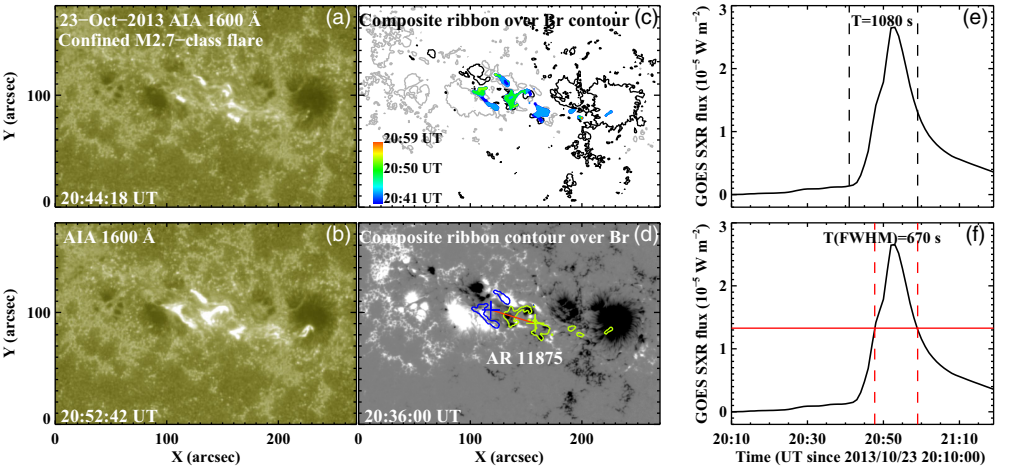

Figure 1. Left: snapshots of the 1600 Å flare ribbons in the M2.7-class confined flare in NOAA AR 11875 observed by AIA on 2013 October 23. Middle: composite ribbons plotted over the Br contours and the positive (blue) and negative (green) contours of composite ribbons over the Br magnetogram. Blue and green pluses respectively denote the positive and negative area-weighted centroids, and the red line in panel (d) represents the ribbon distance. Right: GOES 1-8 Å light curves of this event showing the flare start and end times (dashed lines in panel (e)), and the FWHM duration (panel (f)).

the confined and eruptive events are $1.5{\times}10^{20}$ cm^2 and $1.2{\times}10^{20}$ cm^2 (difference=22%), respectively. The normalized field strength of ARs for confined flares is slightly larger than that for eruptive events (panel (d1)). For ribbon parameters, the reconnection flux and ribbon distance are almost the same for eruptive and confined flares (panels (b2) and d(3)). Confined events have a slightly smaller ribbon area (differences of the log-averages of about 15% in panel (c2)) and have a slightly larger normalized field strength of the ribbon (differences of the log-averages of about 14% in panel (d2)).

In Figures 2(b3) and (c3), we display the histograms of flare reconnection flux ratio (Φ_{ribbon}/Φ_{AR}) and ribbon area ratio (S_{ribbon}/S_{AR}) for confined and eruptive events. It can be seen that the distributions of both flux ratio and area ratio show evident differences, with flux ratio and area ratio for confined events smaller than those for eruptive flares. Reconnection flux ratio ranges between 1% and 41% for eruptive flares and ranges between 1% and 21% for confined events. The log averages of flux ratio are 6.3% for confined and 9.5% for eruptive events. Similarly, the confined flares have the smaller area ratio (1%−18%) than eruptive events (1%−30%). The log-mean values of area ratio R_S are 4.0% for confined and 6.1% for eruptive cases.

Figure 3 shows 6 scatter plots of flare durations versus ribbon parameters for eruptive (blue circles) and confined (red circles) flares. It shows that the FWHM duration has a moderate correlation with ribbon distance, ribbon area and reconnection flux at the correlation coefficients CC of 0.51-0.53 (top in Figure 3). The decay duration also shows a moderate correlation with the two parameters of ribbon distance and reconnection flux at CC of 0.42-0.49 (bottom in Figure 3). The decay duration has a slightly stronger correlation with ribbon area at CC of 0.6 than FWHM duration. These relations are consistent with the results in Toriumi et al. (2017), who showed higher correlation coefficients among these parameters. We suggest that the difference in correlation coefficients is probably due to different ranges of flare classes in different statistical studies.

In our recent work, we extended our database to 722 flares ≥C5.0-class, including 255 eruptive flares and 467 confined events (Li et al. 2021). Figure 4(a) shows the scatter plot

https://doi.org/10.1017/S1743921322004665 Published online by Cambridge University Press

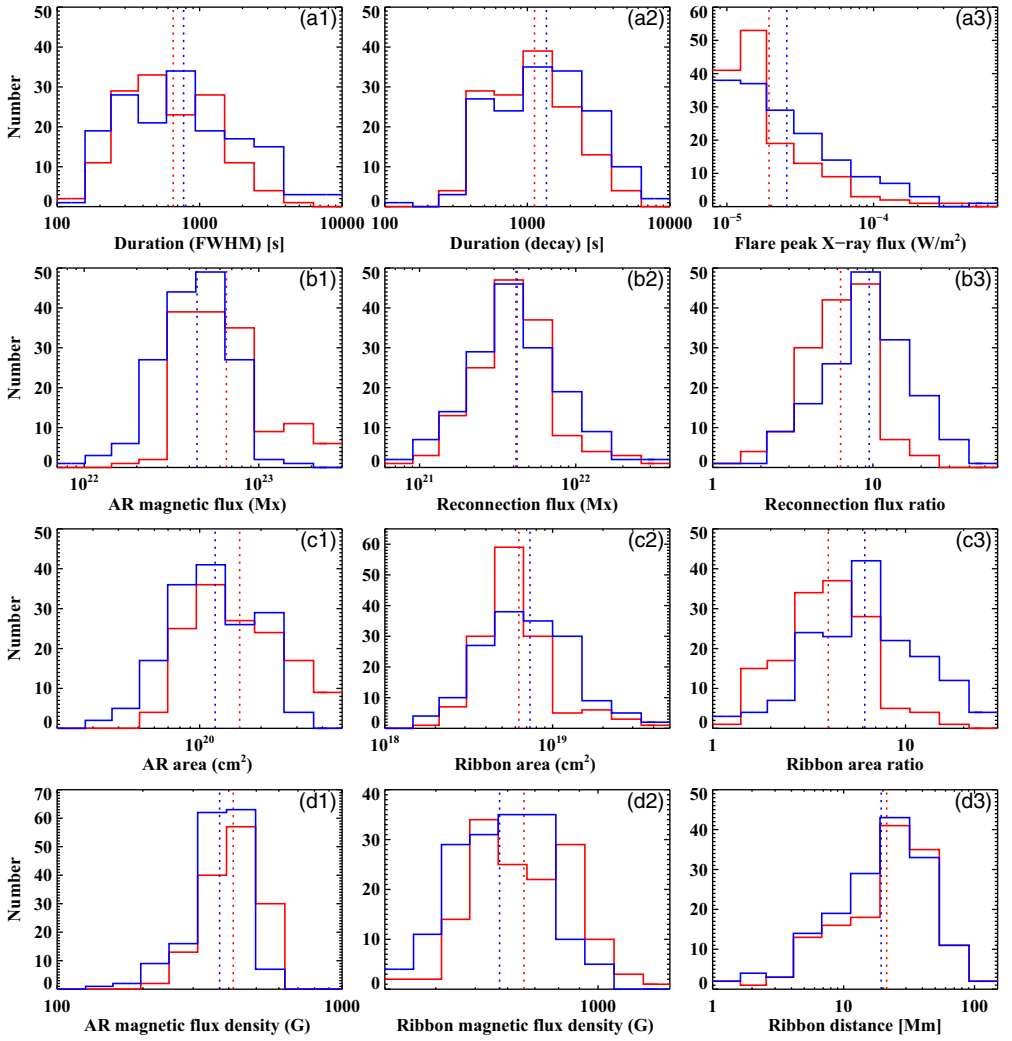

Figure 2. Comparison of the histograms for eruptive (blue) and confined (red) events: total event numbers are 170 and 152, respectively. Dashed vertical lines indicate the means of the log values. Top: histograms of FWHM duration, decay time, and GOES peak flux F_{SXR}. Second row: histograms of AR total magnetic flux Φ_{AR}, ribbon reconnection flux Φ_{ribbon}, and their ratio Φ_{ribbon}/Φ_{AR}. Third row: histograms of AR area S_{AR}, ribbon area S_{ribbon}, and their ratio S_{ribbon}/S_{AR}. Bottom: histograms of normalized field strength of ARs and ribbon areas, and ribbon distance.

of Φ_{AR} versus flare peak SXR flux F_{SXR}. Blue (red) circles are the eruptive (confined) flares. Obviously, when Φ_{AR} is large enough ($> 1.0\times10^{23}$ Mx; horizontal black dashed line), an overwhelming majority (about 97%) of flares do not generate CMEs (57 of 59 flares are confined). The value of Φ_{AR} for the 722 flares ranges from 8.5×10^{21} Mx to 2.3×10^{23} Mx, and we divide Φ_{AR} into 5 subintervals. Figures 4(b)-(f) shows the distributions of eruptive and confined flares in these 5 Φ_{AR} subintervals. It can be seen that in the smallest Φ_{AR} subinterval eruptive flares are not less than confined events, however, this reverses in the largest Φ_{AR} subinterval. Figure 5(a) shows the relations of the CME association rate R with F_{SXR} within the 5 Φ_{AR} subintervals. For each subinterval, R clearly increases with F_{SXR}, similar to previous results that studied the

https://doi.org/10.1017/S1743921322004665 Published online by Cambridge University Press

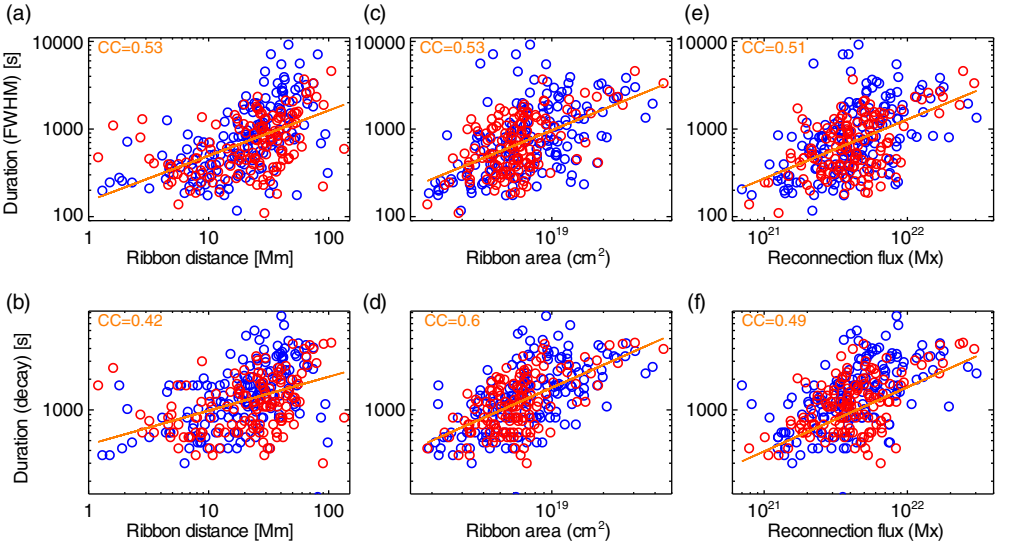

Figure 3. Scatter plots of flare durations versus ribbon parameters for eruptive (blue circles) and confined (red circles) flares. Orange straight line shows the result of a linear fitting to the log−log plots, while correlation coefficient CC is shown at the top left.

CME-flare association as function of flare class during the SOHO era (Yashiro et al. 2006). Each straight line in Figure 5(a) shows the linear fit

$$R = \alpha \log F_{SXR} + \beta, \tag{2.1}$$

where R is in percentage and F_{SXR} is in units of W m^{-2}. For the smallest Φ_{AR} subinterval ($\leq 2.0\times10^{22}$ Mx), the slope α is 113.8±13.1 and R reaches 100% when the flare is larger than M1.3 class (red straight line). For the subinterval of $2.0<\Phi_{AR}\leq3.5\times10^{22}$ Mx, the slope α decreases to 82.0±10.6 and R reaches 100% when the flare is larger than M2.4 class (green straight line). It can be seen that in ARs with a small Φ_{AR}, about 50% C5.0-class flares have associated CMEs. Only about 20% C5.0-class flares have associated CMEs in moderate Φ_{AR} subintervals. In ARs with the largest Φ_{AR} ($> 9.0\times10^{22}$ Mx), R decreases significantly when compared to subintervals characterized by smaller Φ_{AR} (black straight line). The relation between R and F_{SXR} in the largest Φ_{AR} subinterval is

$$R = (22.9 \pm 3.8) \log F_{SXR} + (125.7 \pm 17.9). \tag{2.2}$$

Based on the above equation, only 20% of all M-class flares originating from the largest ARs have associated CMEs and the rate R reaches about 40% for flares >X2. Almost all of C5.0-class flares are confined due to the strong constraining fields in the largest ARs.

Figure 5(b) shows the relation of the slope k with Φ_{AR}. Φ_{AR} is here defined as the mean of the individual log values in each Φ_{AR} subinterval. The plot shows that the slope k decreases monotonically with increasing Φ_{AR}. By assuming ARs in solar-type stars of $\Phi_{AR} \sim 1.0\times10^{24}$ Mx (Maehara et al. 2012; Shibata et al. 2013), and considering a value of the slope $k = 22.9$ in the largest ARs minus the average uncertainty estimates (∼7.8, corresponding to the average error of five diamonds) as the slope k in solar-type stars, we estimate that the slope k might be no more than 15.1±7.8 (red circle). If C5.0-class flares are all confined on solar-type stars (similar to the subinterval of $\Phi_{AR} > 9.0\times10^{22}$ Mx), we can extrapolate the flare-CME association rate for solar-type stars is given as

$$R = (15.1 \pm 7.8) \log F_{SXR} + 80.0. \tag{2.3}$$

https://doi.org/10.1017/S1743921322004665 Published online by Cambridge University Press

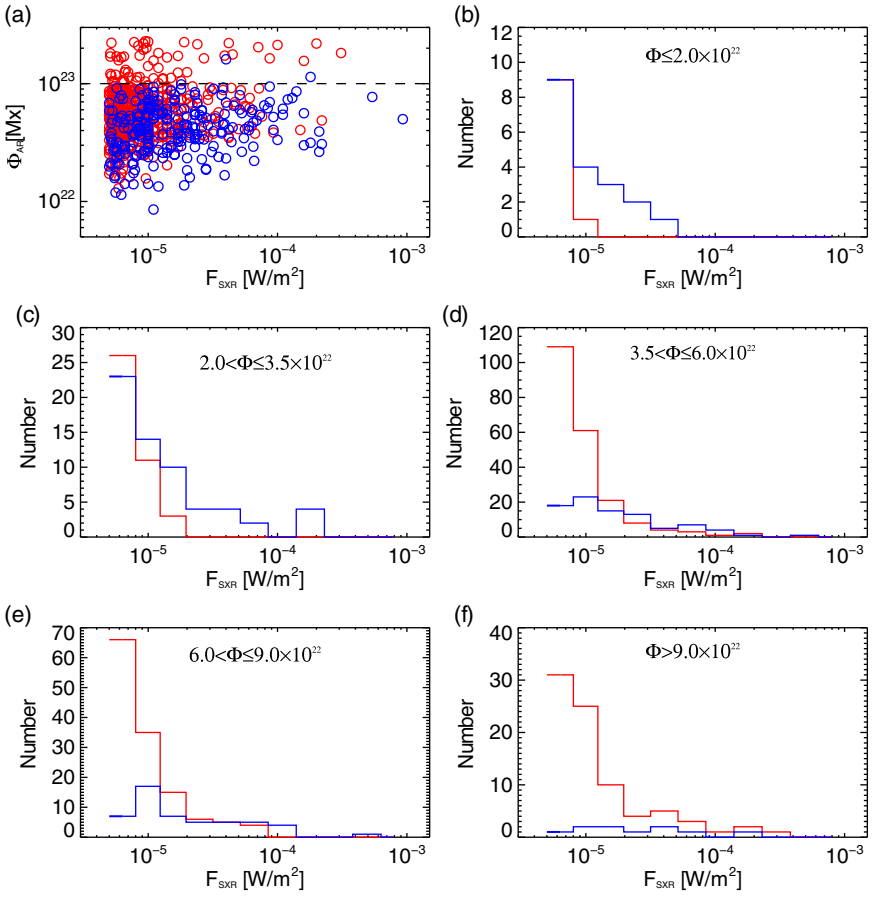

Figure 4. Panel (a): scatter plot of Φ_{AR} vs. F_{SXR}. Blue (red) circles are the eruptive (confined) flares ($\geq$ C5.0-class). Black dashed line corresponds to Φ_{AR} of 1.0×10^{23} Mx. Panels (b)-(f): distributions of eruptive and confined flares in 5 Φ_{AR} subintervals. Blue lines show eruptive flares and red lines show confined events.

Thus, for X100-class superflares in solar-type stars, the estimated association rate R is no more than 50%.

We also estimated the critical decay index heights h_{crit} for 82 events and showed the scatter plot of h_{crit} versus Φ_{AR} in Figure 6(a). It can be seen that h_{crit} increases with Φ_{AR}. This indicates that ARs with a larger magnetic flux tend to have stronger constraining field. The critical decay index height has a strong correlation with AR magnetic flux. The linear fitting to the scatter plot provides the relation of

$$h_{crit} = (38.31 \pm 2.37) \log \Phi_{AR} + (-834.53 \pm 53.92). \quad (2.4)$$

where h_{crit} and Φ_{AR} are in units of [Mm] and [Mx], respectively.

Using this equation, an Φ_{AR} value of 3.0×10^{22} Mx yields a h_{crit} of $\sim$27 Mm (left vertical and bottom horizontal lines in Figure 6(a)) and 1.0×10^{23} Mx corresponds to h_{crit} of about 47 Mm (right vertical and top horizontal lines in Figure 6(a)). In Figure 6(b), we plot the flare peak X-ray flux versus h_{crit}. All flares (28 events) with a h_{crit} value smaller than 27 Mm are eruptive (Area A in Figure 6(b)), and about 95% (20 of 21) of events with h_{crit} larger than 47 Mm are confined (Area C in Figure 6(b)). These results suggest that stronger strapping fields over the ARs with a larger magnetic flux play the major role in confining the eruption.

https://doi.org/10.1017/S1743921322004665 Published online by Cambridge University Press

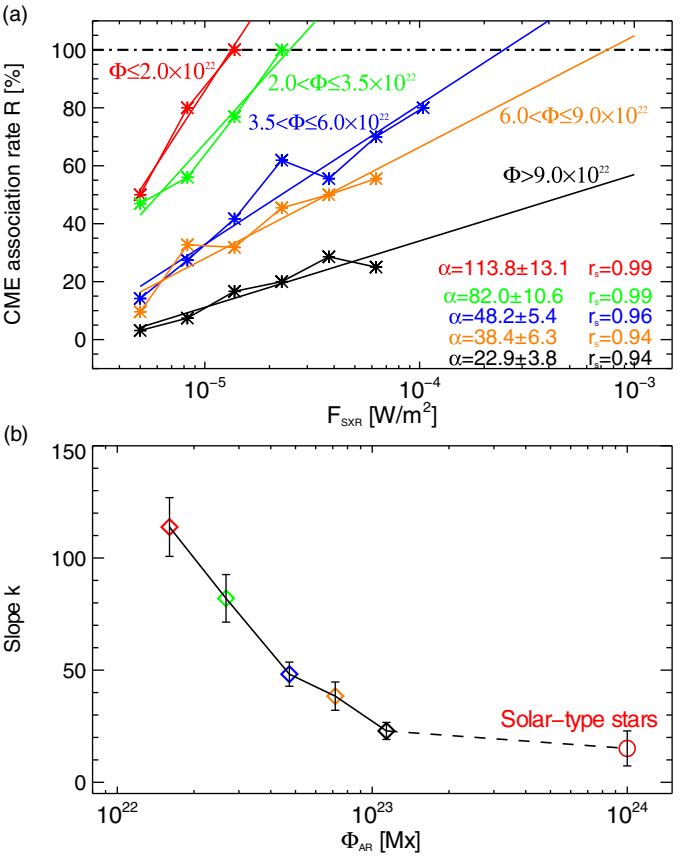

Figure 5. Panel (a): flare-CME association rate R as a function of F_{SXR} separately for 5 different Φ_{AR} subintervals. The colored straight lines show the results of linear fitting, and slopes α and Spearman rank order correlation coefficients r_s are shown at the bottom right. Panel (b): plot of slope k vs. Φ_{AR} (plotted at the average of the log values in each subinterval). Colored diamonds denote the slopes k in five different Φ_{AR} subintervals. The red circle is the estimated value of slope k (about 15.1) for solar-type stars by assuming Φ_{AR} of 1.0×10^{24} Mx (Maehara et al. 2012; Shibata et al. 2013).

We further calculated the magnetic non-potentiality parameters of ARs producing eruptive and confined flares. We use a subset of 106 flare events ≥M1.0 (43 eruptive and 63 confined) from a large database of 322 M-class flares during the period of June 2010 to June 2019 (see details in Li et al. 2022). The subset is selected based on the characteristics of ARs, and the selected ARs must fulfill the following two selection criteria. First, the ARs are flare-active and produced ≥3 M-class flares. Second, the ARs can be unambiguously classified into CME-active and CME-quiet, i.e., all the flares from the same AR have almost the identical eruptive character (ARs with only one exceptional flare event are also selected). A total of 21 ARs fulfill these selection criteria, including 12 CME-active ARs and 9 CME-quiet ARs. Among dozens of non-potential parameters, we select the twist parameter α of the magnetic field, which is the ratio between the vertical current density and the vertical magnetic flux density. For each event, we identified a "flaring polarity inversion line" (FPIL) mask to demarcate the core of an AR by using the method of Sun et al. (2015). We first find the polarity inversion line (PIL) pixels from a smoothed vertical magnetic field B_z, and dilate them with a circular kernel with a radius of 18 pixels (about 6.5 Mm; other radii are also used and the results are not affected).

https://doi.org/10.1017/S1743921322004665 Published online by Cambridge University Press

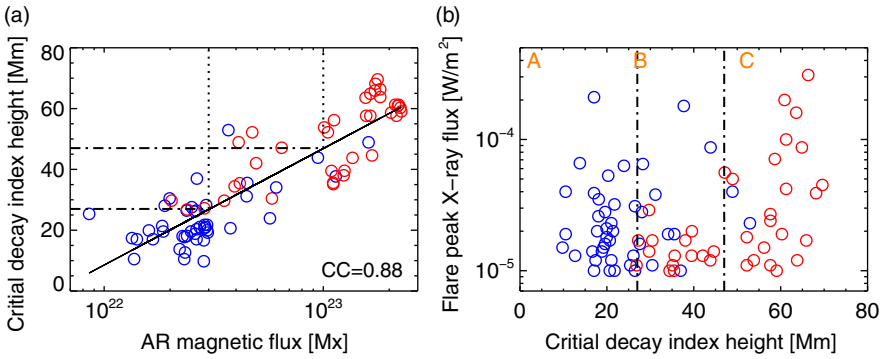

Figure 6. Scatter plots of critical decay index height vs. unsigned AR magnetic flux and flare peak X-ray flux vs. critical decay index height. Blue (red) circles are the eruptive (confined) flares. The black solid line in panel (a) shows the result of a linear fitting, and correlation coefficient CC is shown at the bottom right. Two vertical dotted lines in panel (a) denote the positions where Φ_{AR} respectively equals 3.0×10^{22} Mx and 1.0×10^{23} Mx. Two horizontal dash-dotted lines in panel (a) and two vertical dash-dotted lines in panel (b) respectively refer to critical decay index height of 27 Mm and 47 Mm.

Then we use the 1600 Å image near the flare peak from the AIA on board the *SDO*, and identify the flare ribbon areas by using a large kernel (above 700 DN s^{-1} which is about 10 times the standard deviation above the mean of the quiet-Sun values). Finally the intersection of dilated PIL and ribbon areas is considered as the FPIL mask. We calculate distributions of vertical electric current density J_z and the mean characteristic twist parameter $\alpha_{\rm FPIL}$ within the FPIL mask region.

Figure 7 shows four examples of two eruptive and two confined flares, and includes 1600 Å images (left), photospheric magnetograms (middle) and derived vertical electric current density J_z maps (right). We can see that for two eruptive flares (X2.1 flare in AR 11283 and M6.5 in AR 12371) the positive and negative currents have a coherent structure around the PIL (Figures 7(a)-(b)), indicating the presence of "current ribbons" as in a coherent flux rope. However, the two confined events (X3.1 in AR 12192 and M6.1 in AR 12222) exhibit disordered current distributions and do not have any noticeable structure (Figures 7(c)-(d)). It also can been seen that the FPIL mask regions (orange and black contours) overlap the area of large currents, implying that the FPIL mask corresponds to the AR core with the strongest magnetic non-potentiality.

Based on the derived J_z map, we then calculated the mean characteristic twist parameter $\alpha_{\rm FPIL}$ within the FPIL mask region for the 106 flares. Figure 8(a) shows the scatter plot of $\alpha_{\rm FPIL}$ versus $\Phi_{\rm AR}$. Blue (red) circles are the eruptive (confined) flares. It needs to be noted that $\alpha_{\rm FPIL}$ is a signed parameter and in our study $\alpha_{\rm FPIL}$ means its absolute value. Obviously, for $\alpha_{\rm FPIL}<0.07$ Mm^{-1} (black dotted line in Figure 8(a)), all the flares are confined (a total of 26 confined events). That is, all the eruptive flares have $\alpha_{\rm FPIL}\geq0.07$ Mm^{-1} (a total of 43 eruptive flares). For $\Phi_{\rm AR}<3.5\times10^{22}$ Mx (left green dashed line in Figure 8(a)), all the flares are eruptive. For $\Phi_{\rm AR}>1.0\times10^{23}$ Mx (right green dashed line in Figure 8(a)), all the flares are confined. Figure 8(b) shows the scatter plot of flare peak X-ray flux versus $\alpha_{\rm FPIL}/\Phi_{\rm AR}$. About 93% (40 of 43) of eruptive events have $\alpha_{\rm FPIL}/\Phi_{\rm AR}\geq2.2\times10^{-24}$ Mm^{-1} Mx^{-1}, and $\sim$ 83% (52 of 63) of confined flares have $\alpha_{\rm FPIL}/\Phi_{\rm AR}<2.2\times10^{-24}$ Mm^{-1} Mx^{-1} (black dash-dotted line in Figure 8(b)). This shows that the new relative non-potential parameter $\alpha_{\rm FPIL}/\Phi_{\rm AR}$ is well able to distinguish the two populations of eruptive and confined flares. However, there is still a small overlap (14 of 106) by using our criterion and the exceptional events are mainly from a CME-active AR 11302 and two CME-quiet ARs 11476 and 12268.

https://doi.org/10.1017/S1743921322004665 Published online by Cambridge University Press

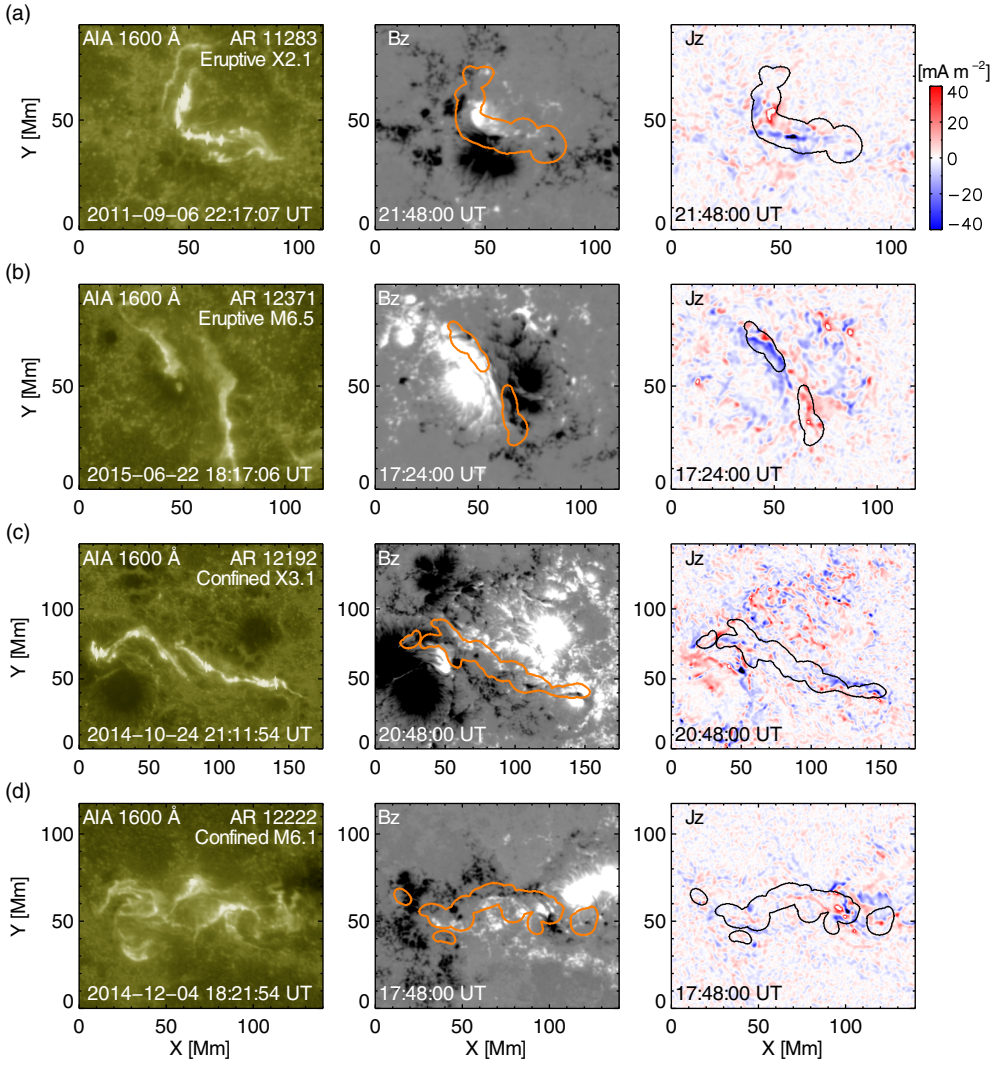

Figure 7. Four examples of two eruptive and two confined flares showing SDO/AIA 1600 Å images (left), SDO/HMI photospheric magnetograms B_z (middle) and derived vertical electric current density J_z maps (right). From top to bottom: eruptive X2.1-class flare in AR 11283, eruptive M6.5-class flare in AR 12371, confined X3.1-class flare in AR 12192 and confined M6.1-class flare in AR 12222. AIA 1600 Å images were remapped with CEA projection. Orange and black contours outline the FPIL mask regions within which the mean characteristic twist parameter ($\alpha_{\rm FPIL}$) in Figure 8 was calculated.

3. Conclusions

Based on the statistical analysis of AR magnetic parameters and ribbon parameters for eruptive and confined flares, our study delivered the following main results.

1. We find that there is no significant difference in distributions of durations and ribbon area between the eruptive and non-eruptive cases (differences of the log-averages of 15%-19%). Flare duration shows a moderate correlation with ribbon area and reconnection magnetic flux at correlation coefficients CC of about 0.5-0.6.

https://doi.org/10.1017/S1743921322004665 Published online by Cambridge University Press

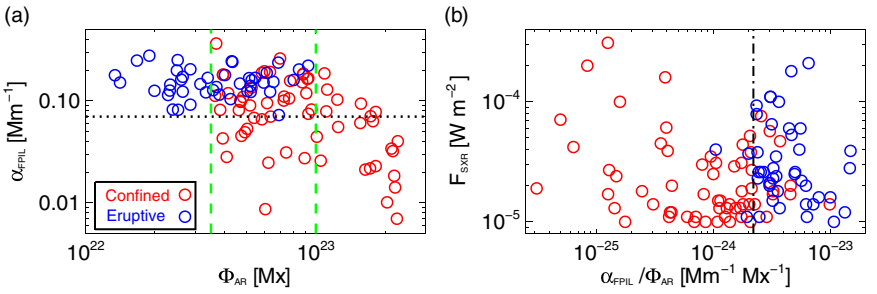

Figure 8. Scatter plots of mean characteristic twist parameter $\alpha_{\rm FPIL}$ versus total unsigned magnetic flux $\Phi_{\rm AR}$ and flare peak X-ray flux $\rm F_{SXR}$ versus $\alpha_{\rm FPIL}/\Phi_{\rm AR}$. Blue (red) circles are eruptive (confined) flares. Two vertical green lines in panel (a) correspond to $\Phi_{\rm AR}$ of $3.5{\times}10^{22}$ Mx and $1.0{\times}10^{23}$ Mx, respectively. The horizontal black line in panel (a) refers to $\alpha_{\rm FPIL}$ of 0.07 Mm^{-1}. The vertical black line in panel (b) denotes $\alpha_{\rm FPIL}/\Phi_{\rm AR}$ of $2.2{\times}10^{-24}$ Mm^{-1} Mx^{-1}.

2. One of the clear differences in distributions for eruptive and confined flares is seen in the total unsigned magnetic flux Φ_{AR} of ARs (difference=39%). When Φ_{AR} is large enough ($> 1.0{\times}10^{23}$ Mx), an overwhelming majority (about 97%) of flares do not generate CMEs (57 of 59 flares are confined). We divided Φ_{AR} into 5 subintervals, and find that the flare-CME association rate R clearly increases with $\rm F_{SXR}$, i.e., larger flares are more likely associated with a CME. The slope of R depends on the total flux of the AR that produces the flare, and reveals a steep monotonic decrease with Φ_{AR}. This means that flares of the same GOES class but originating from an AR of larger Φ_{AR}, are much more likely confined.
3. We also find a very high positive correlation empirical relation between critical decay index height h_{crit} and Φ_{AR}. This implies that ARs with a large magnetic flux have a strong magnetic cage, which confines the eruption.
4. The ratio of the AR magnetic flux that is involved in the flare reconnection process ranges between 1% and 41% for eruptive flares and between 1% and 21% for confined events. Similarly, the confined flares have the smaller area ratio $\rm R_S$ (1%−18%) than eruptive events (1%−30%).
5. By analyzing the mean characteristic twist parameters α_{FPIL} within the "flaring polarity inversion line" region for 106 events, we find that the relative non-potential parameter $\alpha/\Phi_{\rm AR}$ could distinguish effectively between the eruptive from the non-eruptive cases. In about 90% of eruptive flares, $\alpha/\Phi_{\rm AR}$ is beyond the critical value ($2.2{\times}10^{-24}$ Mm^{-1} Mx^{-1}), whereas they are less than the critical value in $\sim$ 80% of confined flares.

In our work, we find that confined flares have similar distributions of duration, ribbon area and ribbon distance compared with eruptive flares. Harra et al. (2016) analyzed 42 X-class flares and found that some X-class eruptive flares showed a very impulsive rise time, and short durations, and some X-class confined flares were long-duration events. Toriumi et al. (2017) showed that there are no obvious differences in duration and ribbon area for eruptive and confined flares. As showed in the standard (CSHKP) flare model, the flare ribbons correspond to the footpoints of newly reconnected post-flare loops. The ribbon distance indicates the footpoint separation of the representative post-flare loop. If the loop configuration does not differ much for different flare events, the loop half length, L, would be proportional to ribbon distance. In the traditional viewpoint, eruptive flare have large-scale hot post-flare loops observed in SXR and are of long duration (e.g., tens of minutes to a few hours), whereas a confined flare shows brightening in compact loop structures that lasts for only a short period (e.g., less than an hour) (Kushwaha et al.

https://doi.org/10.1017/S1743921322004665 Published online by Cambridge University Press

2014; Sahu et al. 2022). Our statistical results are not consistent with the traditional viewpoint, showing that confined flares are not compact and short-duration, and have similar lifetime and spatial scale with eruptive flares.

It was found that flare duration is correlated with magnetic reconnection flux and ribbon area. Toriumi et al. (2017) and Reep & Knizhnik (2019) have also investigated the relationship between the ribbon properties and flare duration. Toriumi et al. (2017) surveyed 51 flare ≥M5.0-class and found the correlation coefficients of flare duration versus reconnection flux and ribbon area are 0.6−0.8, larger than CC (0.5-0.6) in our study. Recently, Reep & Knizhnik (2019) analyzed almost 3000 flares and showed that the duration of GOES light curves is correlated with the magnetic reconnection flux and ribbon area in large flares at the Spearman rank order correlation coefficient r_s of 0.5 and 0.8 for M and X-class flares, respectively. They appear uncorrelated in smaller flares, which is likely due to the large errors in the measurements. It seemed easy to understand the relations: as more magnetic flux is involved, the reconnection processes continue longer.

Our results show that the magnetic flux of ARs is a key parameter in determining the eruptive character of large solar flares, and the flare-CME association rate is decreasing with the increasing magnetic flux of ARs. This finding is further supported by the high correlation obtained between Φ_{AR} and the critical height for torus instability. Φ_{AR} can be considered to be both a measure of the total flux that is in principle available for flaring as well as being a measure of the background field confinement overlying the flaring region. Our findings imply that the latter is the more important factor here. Large Φ_{AR} means a strong confinement and thus the flare-CME association rate is relatively low compared to small Φ_{AR}. Moreover, based on solar observations, we can speculate the associate rate R on solar-type stars by assuming Φ_{AR} of 1.0×10^{24} Mx (Maehara et al. 2012; Shibata et al. 2013). For X100-class "superflares" on solar-type stars, no more than 50% flares can generate stellar CMEs. Our findings provide an important contribution to revise the flare-CME association rates for solar-type stars, by including the distinct differences in these relations in dependence of the AR magnetic flux. This may provide an explanation why the detection of stellar CMEs is rare and the speeds of detected CME candidates are relatively low (e.g. Leitzinger et al. 2014; Veronig et al. 2021; Wu et al. 2022; Lu et al. 2022). Recently, Sun et al. (2022) used the solar magnetic field as a template to estimate the vertical extent of the torus-stable zone above a stellar active region, and suggested that the low apparent CME occurrence rate on cool stars is, at least partially, ascribed to the presence of extended torus-stable zone, which indicates the slowly decreasing confining background coronal magnetic field with height.

Moreover, it is also found that the flux ratio R_{flux} and area ratio R_S for confined flares are significantly smaller than those for eruptive events. This result is similar to the statistical result of Toriumi et al. (2017), who showed the parameter of the ribbon area normalized by the sunspot area determines whether a given flare is eruptive or not. They suggested that the relative structural relation between the flaring region and the entire AR controls the CME productivity.

By considering both the constraining effect of background magnetic fields and the magnetic non-potentiality of ARs, we propose a new parameter $\alpha/\Phi_{\rm AR}$ to describe the eruptive character of a flare, which is well able to distinguish flares associated with CMEs from flares that are not. Parameter α is the average characteristic twist of the magnetic field lines around the PILs of an AR, and provide measures of the nonpotentiality of AR core region (Leka & Skumanich 1999; Benson et al. 2021). Previous studies have shown that the parameter of magnetic twist plays an important role in discriminating between confined and eruptive events and can be used to predict whether an X- or M-class flaring AR would produce a CME (Bobra & Ilonidis 2016; Duan et al. 2019). Magnetic

https://doi.org/10.1017/S1743921322004665 Published online by Cambridge University Press

twist is thought to be related to the driving force of electric current-driven instabilities, such as the helical kink instability (Hood & Priest 1979). An AR containing a highly twisted magnetic field tends to produce an eruption when the twist exceeds a certain threshold. On the other hand, Φ_{AR} has a high positive correlation with the critical decay index height (related to the torus instability of a magnetic flux rope), implying that Φ_{AR} describes the strength of the background field confinement. Our statistical study reveals that the relative parameter α/Φ_{AR} has a better performance in distinguishing between the two types of flares than only Φ_{AR} or α does. We suggest that the relative parameter α/Φ_{AR} indicates the balance between the upward force that drives the eruptions and the downward force that suppresses the eruptions.

Acknowledgements

We are grateful to G. Cauzzi & A. Tritschler for organizing the Symposium IAUS 372. This work is supported by the B-type Strategic Priority Program of the Chinese Academy of Sciences (XDB41000000), the National Natural Science Foundations of China (12222306, 12273060) and Yunnan Academician Workstation of Wang Jingxiu (No. 202005AF150025).

References

Amari, T., Canou, A., Aly, J.-J., et al. 2018, Nature, 554, 211
Avallone, E. A. & Sun, X. 2020, ApJ, 893, 123
Baumgartner, C., Thalmann, J. K., & Veronig, A. M. 2018, ApJ, 853, 105
Benson, B., Pan, W. D., Prasad, A., et al. 2021, SoPh, 296, 163
Bobra, M. G. & Ilonidis, S. 2016, ApJ, 821, 127
Bobra, M. G., Sun, X., Hoeksema, J. T., et al. 2014, SoPh, 289, 3549
Duan, A., Jiang, C., He, W., et al. 2019, ApJ, 884, 73
Fletcher, L., Dennis, B. R., Hudson, H. S., et al. 2011, Space Science Reviews, 159, 19
Gupta, M., Thalmann, J. K., & Veronig, A. M. 2021, A&A, 653, A69
Harra, L. K., Schrijver, C. J., Janvier, M., et al. 2016, SoPh, 291, 1761
Hood, A. W. & Priest, E. R. 1979, SoPh, 64, 303
Kazachenko, M. D., Lynch, B. J., Welsch, B. T., et al. 2017, ApJ, 845, 49
Kazachenko, M. D., Lynch, B. J., Savcheva, A., et al. 2022, ApJ, 926, 56
Kushwaha, U., Joshi, B., Cho, K.-S., et al. 2014, ApJ, 791, 23
Lammer, H., Lichtenegger, H. I. M., Kulikov, Y. N., et al. 2007, Astrobiology, 7, 185
Leitzinger, M., Odert, P., Greimel, R., et al. 2014, MNRAS, 443, 898
Leka, K. D. & Skumanich, A. 1999, SoPh, 188, 3
Li, T., Hou, Y., Yang, S., et al. 2020, ApJ, 900, 128
Li, T., Chen, A., Hou, Y., et al. 2021, ApJ Letters, 917, L29
Li, T., Sun, X., Hou, Y., et al. 2022, ApJ Letters, 926, L14
Liu, L., Wang, Y., Wang, J., et al. 2016, ApJ, 826, 119
Lu, H.-. peng., Tian, H., Zhang, L.-. yun., et al. 2022, A&A, 663, A140
Maehara, H., Shibayama, T., Notsu, S., et al. 2012, Nature, 485, 478
Pesnell, W. D., Thompson, B. J., & Chamberlin, P. C. 2012, Sol. Phys., 275, 3
Reep, J. W. & Knizhnik, K. J. 2019, ApJ, 874, 157
Sahu, S., Joshi, B., Sterling, A. C., et al. 2022, ApJ, 930, 41
Shibata, K., Isobe, H., Hillier, A., et al. 2013, PASJ, 65, 49
Song, Y. & Tian, H. 2018, ApJ, 867, 159
Sun, X., Bobra, M. G., Hoeksema, J. T., et al. 2015, ApJ Letters, 804, L28
Sun, X., Török, T., & DeRosa, M. L. 2022, MNRAS, 509, 5075
Toriumi, S., Schrijver, C. J., Harra, L. K., et al. 2017, ApJ, 834, 56
Török, T. & Kliem, B. 2005, ApJ Letters, 630, L97
Vasantharaju, N., Vemareddy, P., Ravindra, B., et al. 2018, ApJ, 860, 58

Veronig, A. M., Odert, P., Leitzinger, M., et al. 2021, Nature Astronomy
Wang, D., Liu, R., Wang, Y., et al. 2017, ApJ Letters, 843, L9
Wang, Y., & Zhang, J. 2007, ApJ, 665, 1428
Wu, Y., Chen, H., Tian, H., et al. 2022, ApJ, 928, 180
Yashiro, S., Akiyama, S., Gopalswamy, N., et al. 2006, ApJ Letters, 650, L143

https://doi.org/10.1017/S1743921322004665 Published online by Cambridge University Press